# Intrinsic Connectivity Network Disruption in Progressive Supranuclear Palsy

Raquel C. Gardner, MD, Adam L. Boxer, MD, PhD, Andrew Trujillo, BA, Jacob B. Mirsky, MA, Christine C. Guo, PhD, Efstathios D. Gennatas, MBBS, Hilary W. Heuer, PhD, Eric Fine, PhD, Juan Zhou, PhD, Joel H. Kramer, PsyD, Bruce L. Miller, MD, and William W. Seeley, MD

**Objective:** Progressive supranuclear palsy (PSP) has been conceptualized as a large-scale network disruption, but the specific network targeted has not been fully characterized. We sought to delineate the affected network in patients with clinical PSP.
**Methods:** Using task-free functional magnetic resonance imaging, we mapped intrinsic connectivity to the dorsal midbrain tegmentum (dMT), a region that shows focal atrophy in PSP. Two healthy control groups (1 young, 1 older) were used to define and replicate the normal connectivity pattern, and patients with PSP were compared to an independent matched healthy control group on measures of network connectivity.
**Results:** Healthy young and older subjects showed a convergent pattern of connectivity to the dMT, including brainstem, cerebellar, diencephalic, basal ganglia, and cortical regions involved in skeletomotor, oculomotor, and executive control. Patients with PSP showed significant connectivity disruptions within this network, particularly within corticosubcortical and cortico-brainstem interactions. Patients with more severe functional impairment showed lower mean dMT network connectivity scores.
**Interpretation:** This study defines a PSP-related intrinsic connectivity network in the healthy brain and demonstrates the sensitivity of network-based imaging methods to PSP-related physiological and clinical changes.

ANN NEUROL 2013;73:603–616

Progressive supranuclear palsy (PSP) syndrome (PSP-S) presents with progressive gait instability, axial rigidity, ophthalmoparesis, and cognitive–behavioral impairment.[1] Cognitive deficits often occur early and may include executive dysfunction, apraxia of speech, nonfluent aphasia, mental slowing, and cognitive inflexibility.[1–5] Behavioral symptoms, such as apathy, compulsions, obsessions, and utilization/imitation behavior, emerge at varied points along the course.[6] Typical PSP-S (also referred to as Richardson syndrome) features early, prominent gait and oculomotor symptoms that strongly predict underlying PSP pathology, a 4-repeat tauopathy featuring characteristic neuronal and glial tau inclusions in basal ganglia, diencephalon, brainstem, cerebellum, and specific cortical regions.[7–9] In other patients with PSP pathology, cognitive or behavioral deficits arise first and may remain the most conspicuous feature.[9] Consistent with this clinical heterogeneity, PSP pathology is now classified as a subtype of frontotemporal lobar degeneration with tau-immunoreactive inclusions.[10] For clarity, throughout this article we use PSP-S to refer to the typical PSP syndrome and PSP to refer to the histopathological entity.

PSP-S has long been proposed as a network-based disorder.[11–13] This concept rests on the observation that PSP-targeted regions feature robust axonal interconnections in nonhuman primates. The advent of "resting-state" or, perhaps preferably, "task-free" functional magnetic resonance imaging (fMRI) has enabled researchers to identify large-scale intrinsic connectivity networks (ICNs) in humans by mapping regions with temporally correlated low-frequency blood oxygen level-dependent (BOLD) signal fluctuations.[14] ICN mapping has been

View this article online at wileyonlinelibrary.com. DOI: 10.1002/ana.23844
Received Jan 24, 2012, and in revised form Dec 17, 2012. Accepted for publication Dec 21, 2012.
Address correspondence to Dr Seeley, Box 1207, 675 Nelson Rising Lane, Suite 190, San Francisco, CA 94158. E-mail: wseeley@memory.ucsf.edu
From the Memory and Aging Center, Department of Neurology, University of California, San Francisco, San Francisco, CA.
Additional Supporting Information may be found in the online version of this article.

 

used to link healthy human network architectures to the cortically predominant atrophy patterns seen in Alzheimer disease and frontotemporal dementia (FTD).[15,16] Early degeneration in typical PSP-S, however, targets subcortical and brainstem structures[17,18] that have been less well characterized with ICN methods.[19] Because patients with PSP-S often lack severe cortical atrophy,[17,18] cortical dysfunction in PSP-S has been proposed to reflect disconnection of cortical structures from their subcortical inputs and projection targets.[20,21]

We hypothesized that ICN analysis would identify a PSP-related network in healthy subjects and that patients with PSP-S would show connectivity breakdowns within this ICN, even when volumetric changes are incorporated into the analysis. We further sought to explore relationships between connectivity disruption and clinical impairment. Our findings identify a dorsal midbrain-anchored, PSP-related anatomical system in humans and illustrate the sensitivity of ICN methods to network dysfunction and clinical severity in patients with PSP-S.

## Subjects and Methods

### Subjects

*CONTROLS.* Functional and structural MRI scans from 25 young healthy controls (HC1) were acquired from the New York University (NYU) test–retest data set (10 males/15 females; aged 22–49 years; http://www.nitrc.org/frs/?group_id=274) generously made available by Milham and colleagues. As described in the primary publication,[22] these subjects had no history of psychiatric or neurological illness. For our ICN analyses, we used the first scans provided for each NYU subject. To validate our HC1 ICN findings and extend the analysis to healthy older controls, a second healthy control group (HC2) was selected from the University of California, San Francisco (UCSF) Memory and Aging Center database. HC2 consisted of 26 right-handed subjects (13 females) between 60 and 70 years of age. Finally, a third healthy control group (HC3; n=36, 24 females, see Table) was selected for comparison to the PSP-S group. HC3 was composed of 2 healthy control subjects matched to each patient with PSP-S for age, gender, handedness, and education. HC2 and HC3 subjects did not overlap; they were recruited from the San Francisco community through advertisements and underwent a neurological examination and neuropsychiatric assessments as described previously.[23] All were required to have a Clinical Dementia Rating (CDR) scale total score of 0, a Mini-Mental State Examination (MMSE) score of 27 or higher, no significant history of neurological disease or structural lesion on MRI, and a consensus diagnosis of cognitively normal. Diagnoses were rendered within 180 days of MRI scanning in all but 2 subjects, who were diagnosed as cognitively normal within a year prior to and after scanning. Quantitative eye movement evaluation was performed in 24 of the HC3 subjects within 90 days of scanning using methods described previously.[24]

*PATIENTS.* The PSP-S group consisted of 18 patients with a diagnosis of probable PSP based on published consensus clinical diagnostic criteria.[25] This group included all patients in the UCSF database who (1) received a research diagnosis of probable PSP within 180 days of MRI, (2) had undergone task-free fMRI, (3) had no significant history of other neurological disease or structural pathology on MRI (aside from changes consistent with PSP-S), and (4) had measured head movement<3mm translation and 3° rotation. Twenty patients met criteria 1 to 3; 2 were excluded due to excessive movement. Sixteen of 18 patients with PSP-S were taking central nervous system–acting medications at the time of the neuroimaging and clinical evaluations, including 9 patients who were taking dopaminergic medications (see Supplementary Methods for details). Patients underwent a thorough clinical evaluation, including a history, general neurological examination, MMSE, and CDR by a staff behavioral neurologist within 90 days of scanning. Most patients were further evaluated with a bedside neuropsychological screen (n=12), the PSP Rating Scale[26] (PSPRS; n=14), the Unified Parkinson's Disease Rating Scale (UPDRS; n=14), and quantitative eye movement evaluation[24] (n=13), all within 90 days of scanning. A subset of the patients with PSP-S were recruited as part of a pilot clinical treatment trial; all patients, however, underwent MRI before study drug administration. Four of 18 patients studied had died by the time of this writing, and all 4 underwent autopsy. Of these, all 4 had a primary neuropathological diagnosis of PSP.

All subjects or their surrogates provided informed consent prior to participation, and all study procedures were approved by the local institutional review boards.

### Image Acquisition

*NYU DATA SET.* MRI of NYU young healthy controls (HC1) was obtained on a Siemens (Erlangen, Germany) Allegra 3.0T scanner. A T1-weighted magnetization prepared gradient echo (MPRAGE) sequence was also obtained (time to repetition [TR]=2,500 milliseconds, time to echo [TE]=4.35 milliseconds, time to inversion=900 milliseconds, flip angle=8°, 176 slices, field of view=256mm). Task-free fMRI scans were obtained over 6.5 minutes, during which time subjects were instructed to relax with their eyes open, using a T2*-weighted sequence (TR=2,000 milliseconds, TE=25 milliseconds, flip angle=90°, 39 slices, matrix size=64 × 64, field of view=192mm, acquisition voxel size=3 × 3 × 3mm, 197 volumes).

*UCSF DATA SET.* MRI of older controls (HC2 and HC3) and patients with PSP occurred at the UCSF Neuroscience Imaging Center on a Siemens Trio 3.0T scanner. For coregistration purposes, a volumetric MPRAGE MRI sequence was used to obtain a T1-weighted image of the entire brain in sagittal slices during the same session (TR=2,300 milliseconds, TE=2.98 milliseconds, inversion time=900 milliseconds, flip angle=9°). These images

**TABLE. Demographics and Neuropsychological Features for PSP-S and Matched Healthy Controls (HC3)**

| Characteristic | HC3, n=36 | PSP-S, n=18 | *p*, *df* |
|---|---|---|---|
| Age, yr | 68.8 (5.7) | 67.3 (6.0) | 0.394, 52 |
| M:F, No. | 12:24 | 6:12 | NA |
| Education, yr | 16.4 (1.7) | 15.8 (2.6) | 0.312, 54 |
| Illness duration, yr | NA | 4.8 (2.3) | NA |
| PSPRS | NA | 45.0 (13.8) | NA |
| UPDRS | NA | 37.5 (15.1) | NA |
| Downward saccade velocity, °/s | 340.3 (85.5) | 90.0 (65.3) | <0.001, 35 |
| CDR, total | 0 (0) | 0.94 (0.6) | NA |
| CDR, sum of boxes | 0.01 (0.08) | 5.9 (3.7) | NA |
| MMSE, max=30 | 29.5 (0.8) | 26.1 (4.5) | <0.001, 54 |
| CVLT-SF, 4 learning trials, total, max=36 | NC | 18.5 (11.7) | NA |
| CVLT-SF, 10-minute recall, score, max=9 | NC | 4.2 (3.0) | NA |
| Modified Rey-O copy, max=17 | 15.3 (0.9) | 11.4 (4.2) | <0.001, 34 |
| Modified Rey-O 10-minute recall, max=17 | 12.6 (2.6) | 8.4 (3.7) | 0.001, 27 |
| Digit span backward | 5.5 (1.4) | 3.6 (0.9) | <0.001, 39.4 |
| Modified trails, correct lines per minute | 36.9 (11.6) | 13.8 (6.4) | <0.001, 47 |
| Design fluency, max=30 | 10.9 (3.7) | 5.8 (2.3) | <0.001, 45 |
| Letter fluency, D words in 1 minute | 15.5 (5.0) | 6.6 (4.8) | <0.001, 40 |
| Semantic fluency, animals in 1 minute | 23.6 (5.3) | 10.0 (4.8) | <0.001, 48 |
| Abbreviated BNT, max=15 | 14.7 (0.6) | 13.6 (2.2) | 0.015, 50 |
| Calculations, max=5 | 4.9 (0.3) | 3.9 (0.8) | <0.001, 47 |
| Translational motion, mRMS, mm | 0.33 (0.19) | 0.33 (0.28) | 0.52, 54 |
| Rotational motion, mEuler | 0.13° (0.09°) | 0.16° (0.15°) | 0.96, 54 |

Values represent mean (standard deviation). Nonparametric tests were used where appropriate.
BNT=Boston Naming Test; CDR=Clinical Dementia Rating; CVLT-SF=California Verbal Learning Test–short form; F=female; M=male; mEuler=mean Euler angle; MMSE=Mini-Mental State Examination; mRMS=mean root mean square; NA=not applicable; NC=not collected; PSP=progressive supranuclear palsy; PSPRS=PSP Rating Scale; UPDRS=Unified Parkinson's Disease Rating Scale.

were reconstructed as a 160 × 240 × 256 matrix with $1mm^3$ spatial resolution. Task-free fMRI images were obtained using an 8-minute T2*-weighted sequence, during which subjects were instructed to remain awake with their eyes closed. Thirty-six interleaved axial slices (3mm thick including a gap of 0.6mm) were imaged parallel to the plane connecting the anterior and posterior commissures using a T2*-weighted echo planar imaging sequence (TR=2,000 milliseconds, TE=27 milliseconds, flip angle=80°, field of view=230 × $230mm^2$, matrix size=92 × 92; in-plane voxel size=2.5 × 2.5mm) with an online gradient adjustment for head motion compensation.

### *Image Preprocessing and Analysis*

*STRUCTURAL IMAGING.* Using the SPM8 VBM8 (University College London, London, UK) toolbox, the PSP-S and HC3 T1-weighted images were processed using the VBM8 default estimation settings, segmented into gray and white matter, spatially normalized with the SPM8 default low-dimensional spatial normalization, subjected to a light cleanup (to remove any remaining non–brain tissue from the data), modulated, corrected for nonlinear warping only, and smoothed with a 12mm full width at half maximum isotropic Gaussian kernel. Correction for total intracranial volume was not performed as nonlinear modulation and normalization corrects for variations in brain size. The resulting gray and white matter maps were subsequently used to assess the atrophy pattern in our PSP-S group, model the effects of brain structure on intrinsic connectivity in PSP-S, and compare the utility of ICN and voxel-based morphometry (VBM) approaches for detecting PSP-S–related changes.

*FUNCTIONAL IMAGING: HEAD MOTION ASSESSMENT.* Subject head motion was assessed by using the rigid body parameters provided by the realign algorithm in SPM5. Parameters for a given volume in the time series were compared to the parameters for the previous volume, creating a set of values that captured the amplitude of volume-to-volume changes. Using these values, mean root-mean-square values were calculated for translation and mean Euler angles for rotation, as these summary metrics have been shown to correlate with network connectivity strength.[27] The PSP-S and HC3 groups showed no significant differences in translational or rotational movement (see Table).

*FUNCTIONAL IMAGING: PREPROCESSING AND REGION OF INTEREST–BASED INTRINSIC CONNECTIVITY ANALYSIS.* Using SPM5, UCSF subjects' functional images were spatially realigned, slice time corrected, coregistered to each subject's structural T1-weighted image, normalized to the Montreal Neurological Institute T1 template, and smoothed with a 4mm Gaussian kernel. Handling of NYU images was identical except that the functional images were normalized directly to the SPM5 EPI template.

Consistent with our previous approaches,[15] we selected a seed for the region of interest (ROI)-based ICN analysis from regions shown to be significantly atrophied in a VBM study performed at our center on an independent (nonoverlapping) group of patients with PSP-S.[17] Among the 6 gray matter regions previously identified, we selected the dorsal midbrain tegmentum (dMT) because, in contrast to the other regions, the dMT was seated further from the subarachnoid space (mitigating concerns regarding mixed tissue compartment signals) and fell within a region imaged in all subjects (unlike the pontine tegmentum region, which fell partly outside the inferior edge of the task-free fMRI bounding box for some subjects). Further supporting this seed choice, recent clinicoanatomical studies have shown that dMT volume correlates with vertical saccade velocity, a function classically impaired in typical PSP-S.[24] The dMT ROI consisted of a 4mm-radius sphere centered at the local maximum from the previous VBM study comparing PSP-S to controls (5, −15, −8).[17] Using SPM8, we calculated the average BOLD signal intensity of all voxels within this ROI at each TR over each subject's 8-minute scan. We used the resulting time series as a covariate of interest in a whole-brain statistical parametric regression analysis to derive images corresponding to the dMT intrinsic functional correlation map for each subject. A total of six 4mm-radius spherical ROIs embedded in the cerebrospinal fluid (CSF; left posterior and right anterior lateral ventricles) and white matter (left and right frontal and left and right parietal corona radiata) were included as covariates to reduce effects of physiological noise. We omitted the global signal and motion parameters as nuisance covariates based on recent work showing that inclusion of these measures exerts a negative effect (global signal regression) or no effect (motion parameters) on ICN test–retest reliability[28] and may unnecessarily reduce fMRI signal (motion parameters).[29] One-sample $t$ tests were performed separately in HC1 and HC2 to identify clusters with significant intrinsic connectivity to the dMT in healthy young and older subjects at a cluster-forming height threshold of $p < 0.0001$ uncorrected and a cluster extent threshold of $p < 0.001$ corrected for familywise error. To identify smaller brainstem and subcortical regions with highly significant correlation to the dMT, we also visualized the HC1, HC2, and HC1/HC2 overlap maps at a voxel-level, familywise error-corrected threshold of $p < 0.05$ (no extent threshold). We employed this rigorous discovery (HC1) and replication (HC2) strategy because few previous ROI-based ICN studies have focused on brainstem ROIs and to ensure that the novel ICN delineated here showed topographical consistency across the adult age spectrum, consistent with other more extensively studied ICNs.[30,31]

To compare the strength of the dMT-associated ICN in PSP-S to that in healthy matched controls (HC3), we entered the PSP-S and HC3 subject-level ICN maps into a second-level, random effects analysis masked to voxels for which nonzero fMRI signal was present in all subjects (to avoid including brainstem regions covered in some but not all subjects). Two-sample $t$ tests were performed to evaluate linear contrasts representing PSP-S<HC3 and PSP-S>HC3. Next, we used the BPM toolbox[32] to enter each subject's VBM gray and white matter maps as voxelwise covariates to control for the effects of atrophy on ICN strength. Results of atrophy-uncorrected and corrected 2-sample $t$ tests were thresholded using joint probability distribution thresholding[33] with joint height and extent thresholds of $p < 0.01$ and $p < 0.05$ (for visualization purposes), corrected across the search volume, in keeping with our previous work.[34] For these analyses, we applied an explicit dMT-seeded ICN mask, derived from the HC2 group 1-sample $t$ test (voxel height threshold of $p < 0.005$ uncorrected, extent threshold of $p < 0.01$), chosen to generously constrain the search volume to regions within the dMT-associated ICN.

*FUNCTIONAL IMAGING: ICN NODE PAIR MATRIX-BASED ANALYSIS AND GRAPH THEORETICAL METRICS.* Because the seed ROI-based method only provides information about each voxel's connectivity to the chosen seed ROI, we used the HC2-derived dMT-seeded ICN, to create a group of intrinsic connectivity clusters for an ROI matrix-based analysis, allowing us to examine all pairwise ROI interactions. Cluster ROI creation followed methods described in the Supplementary Materials. The mean voxelwise BOLD signal time series for each resulting ROI was used to create partial correlation matrices, with all other ROIs, that represent the ROI pairwise correlation coefficients after controlling for white matter and CSF nuisance regressors. These group-level pairwise correlations were visualized as matrices to facilitate assessment of connectivity reduction patterns in PSP-S. Two-sample $t$ tests identified ROI pairwise differences in intrinsic connectivity between the PSP-S and HC3 groups, thresholded using false discovery rate correction for multiple comparisons at $p < 0.05$.

To augment the matrix-based ICN analyses described above, we used the methods of graph theory[35] to further characterize the normal network architecture and to derive metrics for group-level contrasts. In graph theoretical terms, each ROI

represents a node, and the connectivity between each pair of ROIs represents an edge. We used the ICN matrices from the HC2 group to generate a graph in Cytoscape (http://www.cytoscape.org) based on an edge-weighted, force-directed layout algorithm that configures the nodes in space according to the weights of their edges, in this case based on the node pair correlation coefficients transformed to $z$ scores and thresholded at $z>0.31$ ($r=0.3$). To gauge the sensitivity of network architecture to matrix thresholding, we generated 2 further graphs, 1 with a more lenient and another with a more stringent threshold (Supplementary Fig 3).

To further explore differences between PSP and HC3 with regard to network architecture, we calculated total flow, mean clustering coefficient, and mean path length from the adjacency matrices for each subject, thresholded using the same 3 thresholds used to generate the HC2 graphs. Total flow is a measure of weighted degree, computed as the sum of a node's weighted pairwise connections. Clustering coefficient is a node-wise metric that captures the degree to which a node's first-level neighbors are connected to each other. Path length describes the shortest connectional distance required to travel between 2 given nodes in the graph. Two-sample $t$ tests were used to compare nodal total flow and clustering coefficient values between PSP-S and HC3, thresholded using false discovery rate correction for multiple comparisons at $p < 0.05$. Mean total flow, clustering coefficient, and path length were compared between groups using Mann–Whitney $U$ tests performed for each HC2 graph threshold. Equations used to calculate graph metrics were implemented in Matlab using the Brain Connectivity Toolbox and MatlabBGL (http://www.cs.purdue.edu/homes/dgleich/packages/matlab_bgl/).[36]

*CORRELATION BETWEEN DMT-ASSOCIATED ICN CONNECTIVITY AND CLINICAL SEVERITY.* To assess the relationship between PSP-S clinical severity and intrinsic connectivity, we derived a dMT-asociated ICN score for each patient with PSP-S. This score was computed as the mean beta value across all voxels of each subject's dMT-associated ICN map within an HC2-derived dMT network mask (thresholded at a joint height and extent threshold of $p < 0.001$). Because the resulting ICN scores were non-normally distributed within the PSP-S group, we used Spearman correlation to examine the relationship between mean dMT ICN score and CDR sum of boxes, UPDRS, and PSPRS. These clinical measures were chosen because they summarize clinical severity in PSP and showed ample dynamic range without floor or ceiling effects. In addition, we examined Spearman correlations between mean dMT ICN score and vertical saccade velocity, measured in degrees per second. Age, gender, and movement parameters showed no significant correlation with the dMT-associated ICN score, and these potential confounders were therefore omitted from the analyses to improve power.

*COMPARISONS BETWEEN ICN AND VBM FINDINGS IN PSP-S.* In an exploratory analysis, we compared the sensitivity of task-free fMRI and VBM analyses for detecting network degeneration in PSP-S. At each voxel, effect size for the PSP<HC3 contrast was calculated using voxelwise group means and pooled standard deviations derived from the subject-level ICN or VBM gray matter maps. Maps were created to visualize where ICN analysis generated a greater effect size than VBM and vice versa (see Supplementary Methods).

*STATISTICAL THRESHOLDING PRINCIPLES FOR IMAGE ANALYSES.* A consistent thresholding strategy was used for the primary imaging analyses. One-sample $t$ tests for network definition were thresholded at a cluster-forming height threshold of $p < 0.0001$ and a cluster extent threshold of $p < 0.001$ corrected for familywise error across the whole brain. Major study hypotheses (2-sample $t$ tests comparing PSP-S to HC3) were tested at a joint height and extent threshold of $p < 0.01$ as well as $p < 0.05$ (for visualization purposes), cluster-level corrected across the search volume.[33] Thresholds not used for hypothesis testing were guided by their specific purpose. For example, network masks were thresholded to generously constrain group-level analyses to a specific ICN without expanding the search volume to the entire brain.

## Results

### The Healthy Brain Features an ICN Composed of PSP-Vulnerable Brain Regions

Our first goal was to identify a healthy brain network composed of regions known to degenerate in PSP-S. To pursue this objective, we conducted ICN analyses in 2 independent healthy control groups (young [HC1] and older [HC2] controls). Using ROI-based task-free fMRI analysis, we identified regions that showed significant intrinsic connectivity with the dMT, a primary focus of gray matter atrophy in PSP-S[17] that correlates with vertical saccade velocity in patients with PSP-S and other neurodegenerative disorders.[24] As expected, the ICNs converged in the healthy young and older control network discovery and replication groups (HC1 and HC2; Fig 1). Despite seeding this ICN analysis with a focal midbrain ROI, we detected a distributed network pattern that included additional brainstem, cerebellar, diencephalic, basal ganglia, and cortical regions known to degenerate along differing gradients in typical and atypical PSP-S,[9] and to cooperate in the healthy brain to support skeletal and ocular motor function, gait, action planning, and cognitive–behavioral control. Because prominent behavioral and speech praxis deficits can accompany typical PSP-S, we noted with interest that the dMT-associated ICN also included the pregenual anterior cingulate and frontoinsular cortices, which show early degeneration in the behavioral variant of FTD (bvFTD),[37] as well as the frontal operculum/dorsal anterior insula, a focus of atrophy in patients with nonfluent aphasia and apraxia of speech.[38] Importantly, the dMT-associated ICN was consistent across different adult age groups, scanners, and acquisition protocols, confirming that it represents a robust and reproducible ICN.

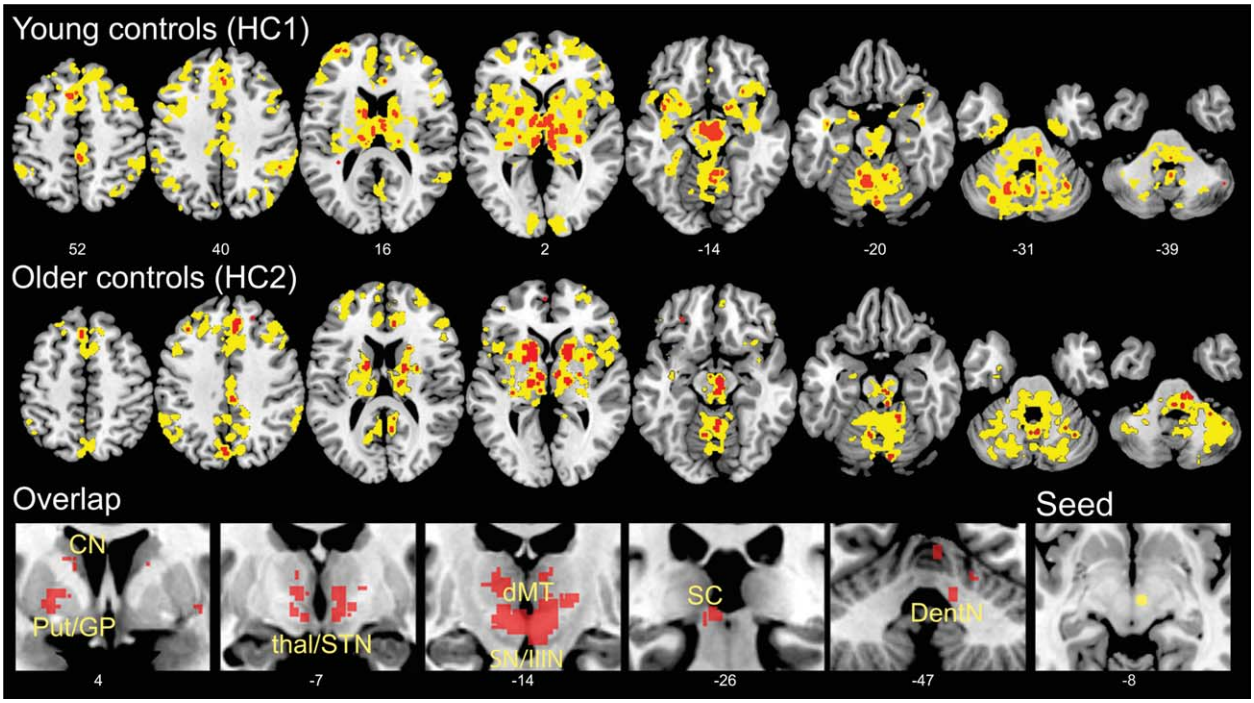


**FIGURE 1: The dorsal midbrain tegmentum (dMT)-associated intrinsic connectivity network (ICN). The dMT was used as a seed region of interest for voxelwise task-free functional magnetic resonance imaging analyses in healthy young (HC1, upper row) and older (HC2, middle row) controls. Results are displayed at height threshold $p<0.0001$, extent threshold $p<0.001$ familywise error corrected at the cluster level (yellow) and at height threshold $p<0.05$, familywise error corrected at the voxel level (red) to avoid omitting small but significant brainstem clusters. Corrections were performed across the whole brain. The overlap between the voxel level results for the 2 control groups (bottom row) is shown to highlight the consistency of the pattern within subcortical, diencephalic, and brainstem/cerebellar structures central to the known progressive supranuclear palsy pathological injury pattern. The rightmost panel in the bottom row shows an axial view of the dMT seed (yellow) used for the seed-based ICN analysis. Slice labels reflect Montreal Neurological Institute coordinates. The right side of the images corresponds to the right side of the brain. CN=caudate nucleus; DentN=dentate nucleus; GP=globus pallidus; IIIN=third nerve nuclear complex; Put=putamen; SC=superior colliculus; SN=substantia nigra; STN=subthalamic nucleus; thal=thalamus.**

### *PSP-S Is Associated with Reduced Connectivity throughout the dMT-Associated ICN*

Next, we sought network connectivity changes in patients with PSP-S. Compared to 36 matched healthy controls (HC3), patients with PSP-S showed distributed network connectivity reductions throughout the dMT-seeded ICN (Fig 2, Supplementary Table 1), most prominent in striatum, thalamus, cerebellum, and cortical regions. Omitting the dMT-associated network mask revealed minimal changes; a few clusters of reduced connectivity in PSP-S extended just beyond the mask boundaries or into contiguous regions, such as the superior and middle temporal gyri. Importantly, no regions of increased connectivity were identified in PSP-S versus controls (with or without masking) even at the lower statistical threshold included in Figure 2 for visualization purposes. After atrophy correction, the PSP-S<HC3 contrast differed little, with only the dorsal midbrain and supplementary motor area (SMA) showing less extensive dMT connectivity reduction in PSP-S (Supplementary Fig 2). No regions of increased connectivity in PSP-S were identified in the atrophy-corrected model.

### *PSP-S Is Associated with Distributed Node Pair Connectivity Reductions throughout the Dorsal Midbrain Tegmentum-Associated ICN Matrix*

To map a more comprehensive network architecture among the regions identified with the seed ROI-based approach, we created data-driven ROIs representing the major nodes of the dMT-associated ICN (Fig 3, Supplementary Fig 1, Supplementary Table 2; clusters available upon request from the corresponding author). PSP-S showed pairwise connectivity reductions distributed throughout this matrix (see Fig 3E), especially in cortico-subcortical and cortico-brainstem connections. No node pair connection showed increased connectivity. This analysis extended the seed-based ICN findings by showing that regions distributed throughout this neural system show reduced connectivity with each other, not only with the dMT.

The healthy configuration of the fully specified network is graphed in Figure 4 using an edge-weighted, force-directed algorithm to capture nodes' relationships with each other. This approach illustrated the centrality of the mesothalamic junction (MTJ; just rostral to the dMT), basal ganglia (a cluster spanning anterior caudate,

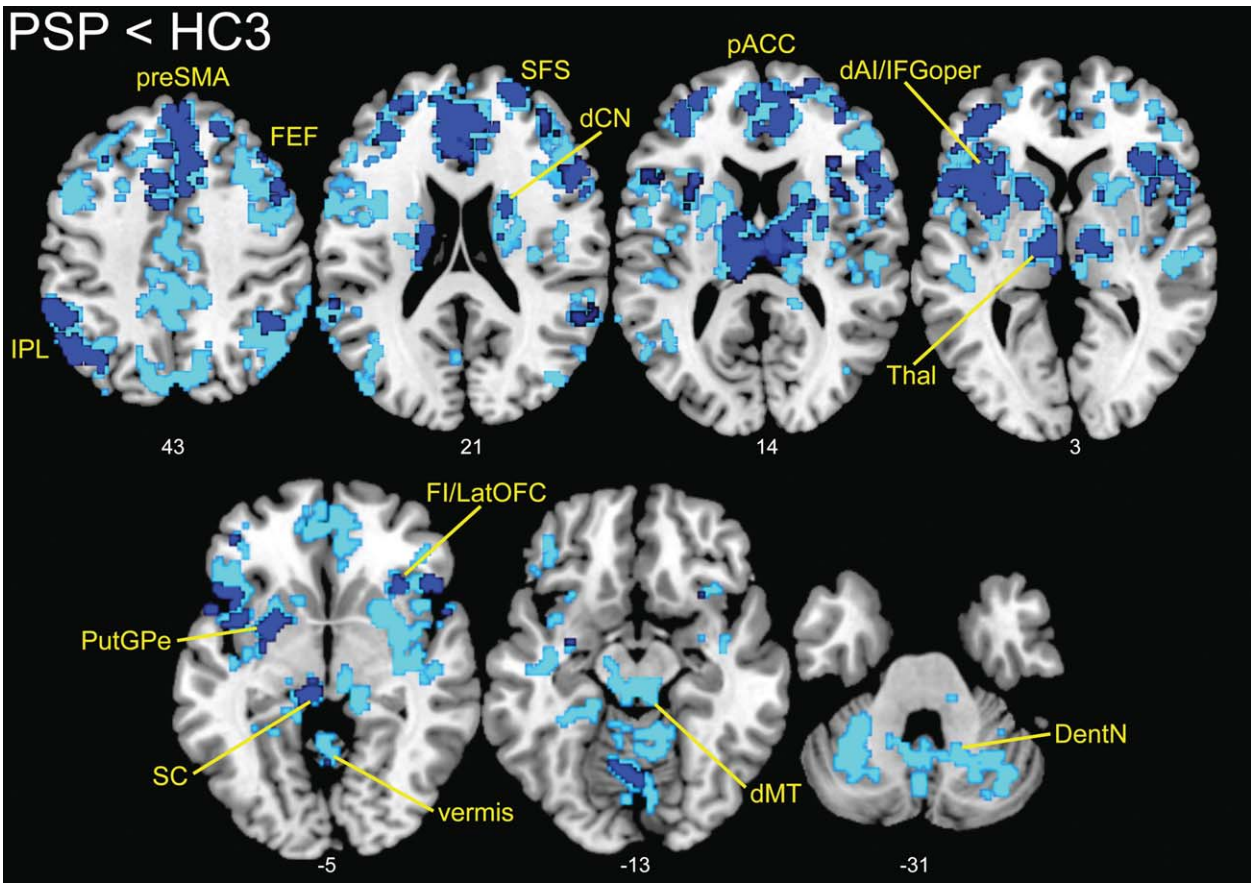


**FIGURE 2: Network connectivity reductions in progressive supranuclear palsy syndrome (PSP-S). Examining the same dorsal midbrain tegmentum (dMT)-associated intrinsic connectivity network shown in Figure 1, we found connectivity reductions in PSP distributed throughout the network. Results are displayed at $p<0.01$ (dark blue) and $p<0.05$ (light blue), joint height and extent corrected at the cluster level across the network. Slice labels reflect Montreal Neurological Institute coordinates. The right side of the images corresponds to the right side of the brain. dAI=dorsal anterior insula; dCN=dorsal caudate nucleus; DentN=dentate nucleus; FEF=frontal eye fields; IFGoper=inferior frontal gyrus (pars opercularis); FI=frontoinsula; GPe=globus pallidus externa; IPL=inferior parietal lobule; LatOFC=lateral orbitofrontal cortex; pACC=pregenual anterior cingulate cortex; preSMA=pre–supplementary motor area. Put=putamen; SC=superior colliculus; SFS=superior frontal sulcus; Thal=thalamus.**

putamen, and pallidum), and thalamus. These hublike nodes feature high-degree centrality and provide a functional link between the cortex and brainstem/cerebellum. Comparing each node's total flow (the sum of its weighted edges) in PSP-S and HC3, we identified the MTJ and several key cortical regions as showing significant total flow reductions in PSP-S (see Fig 4). All network nodes showed reduced clustering coefficients in PSP-S (false discovery rate–corrected, $p < 0.05$). Mean total flow and clustering coefficient (computed across all nodes) showed significant reductions in PSP-S (Supplementary Table 3). No significant differences were found for mean path length at any of the 3 HC2 graph thresholds.

### *PSP-S Connectivity Reductions Correlate with Clinical Impairment*

To explore whether ICN measures prove sensitive to disease severity, we assessed correlations between the mean dMT-associated ICN score (see Subjects and Methods) and clinical measures that summarize functional integrity. Initially, no significant correlations were found. Examination of these data, however, revealed 1 conspicuous outlier: a patient with PSP-S having severe clinical impairment despite a relatively high mean dMT-associated ICN score. Excluding this outlier recovered a significant inverse relationship between mean dMT-associated ICN strength and the CDR sum of boxes score ($\rho=-0.662$, $p=0.004$; Fig 5), indicating that patients with more advanced disease showed weaker network connectivity. Similar but nonsignificant negative correlations were seen for the PSPRS ($\rho=-0.345$, $p=0.249$) and UPDRS ($\rho=-0.319$, $p=0.288$) with the outlier excluded. We further observed a trend toward slower downward saccades in patients with lower ICN scores ($\rho=0.511$, $p=0.074$; outlier included). Importantly, patients with PSP-S who were or were not taking dopaminergic agents showed no difference in mean dMT connectivity ($t=0.409$, $p=0.688$), a finding that held after

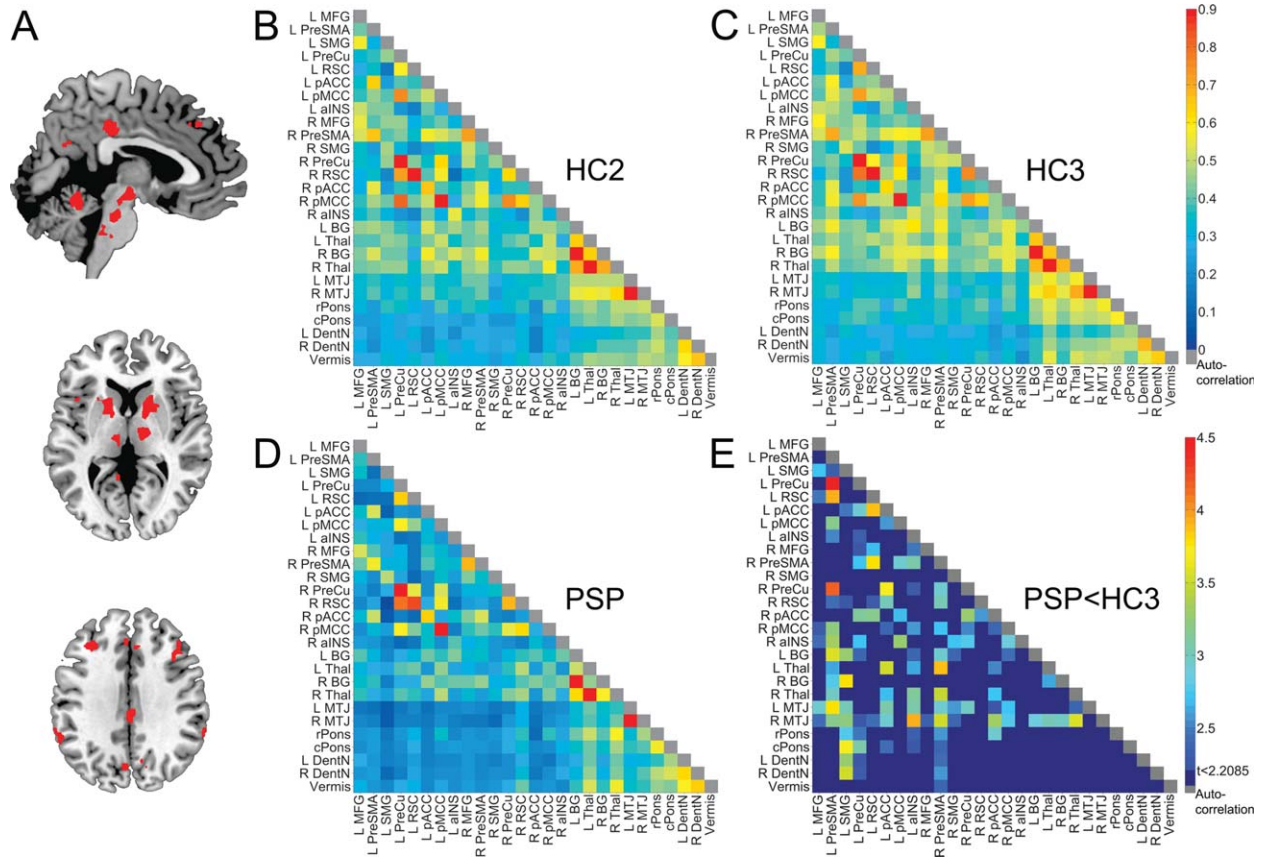


**FIGURE 3: The broader progressive supranuclear palsy (PSP)-related network in health and disease. Regions showing intrinsic connectivity to the dorsal midbrain tegmentum in the HC2 group were isolated (A; Supplementary Fig 1, Supplementary Table 2) and used to generate matrices representing the connectivity strength between each region-of-interest pair for HC2 (B), HC3 (C), and PSP (D). The Color bar in C applies to B through D and indicates the Pearson correlation coefficients *(r)* derived for each node pair transformed to *z* scores. (E) The node pair matrix highlights those pairs showing significant connectivity reduction in PSP versus HC3, corrected at the matrix level for false discovery rate to produce a $p<0.05$ ($z\geq2.21$). The color bar indicates the *z* scores derived from the 2-sample *t* test (PSP<HC3). Colored node pairs indicate significant reductions. aINS=anterior insula; BG=basal ganglia; cPONS=caudal pons; DentN=dentate nucleus; L=left; MFG=middle frontal gyrus; MTJ=mesothalamic junction; pACC=pregenual anterior cingulate cortex; pMCC=posterior midcingulate cortex; PreCu=precuneus; PreSMA=pre–supplementary motor area; R=right; RSC=retrosplenial cortex; SMG=supramarginal gyrus; Thal=thalamus.**

exclusion of the outlier in the connectivity–behavior correlation analyses, who was taking carbidopa/L-dopa ($t=0.942$, $p=0.361$).

### *Intrinsic Connectivity and Morphometric Analyses Play Complementary Roles in Detecting Network Degeneration in PSP-S*

Early detection and disease-monitoring PSP-S biomarkers may need to detect physiological changes that precede gross atrophy. We hypothesized that ICN analysis would prove more sensitive to early disease in regions with little or no atrophy, whereas structural imaging (VBM), which involves less methodological noise, would outperform ICN methods in regions already showing significant atrophy. To test these ideas, we used the PSP-S<HC3 contrasts to compare the voxelwise effect sizes of dMT connectivity reduction to those derived from VBM. As predicted, we found that dMT connectivity showed larger effect sizes in network regions functionally connected to areas where significant atrophy had already emerged. Conversely, VBM generally produced larger effect sizes for regions already showing significant atrophy (Fig 6). These findings suggest that ICN and VBM approaches may provide complementary information and raise the speculation that ICN mapping may prove most valuable during early stage disease.

## Discussion

This study establishes an ICN, anchored by the dorsal midbrain, whose nodes include the brainstem, basal ganglia, diencephalic, cerebellar, and cortical regions that show atrophy and tau aggregation in PSP.[1,9,17] Hence, PSP-S, like other neurodegenerative disease syndromes,[15] reflects injury to a specific large-scale cortical–subcortical system that can be mapped in the healthy brain with

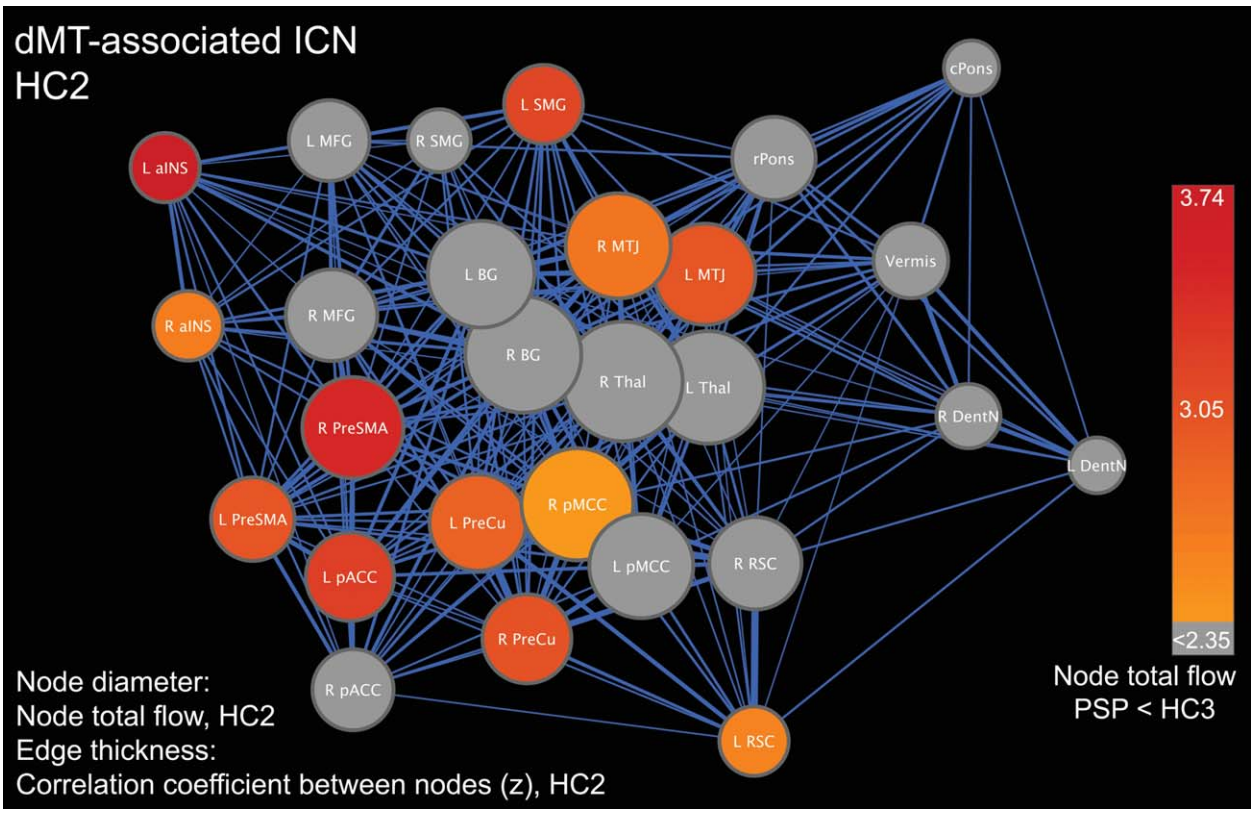


**FIGURE 4: The matrix-derived dorsal midbrain tegmentum (dMT)-associated intrinsic connectivity network (ICN) architecture and connectivity reductions in progressive supranuclear palsy syndrome (PSP-S). An edge-weighted force-directed algorithm was used to display the relationships among network nodes in the healthy brain (HC2 data). Heuristically, nodes clustered together represent more closely related subnetworks, and nodes placed centrally within the overall graph have stronger, more numerous edges characteristic of central hubs. Node diameter represents node total flow, whereas edge thickness represents the correlation coefficient (transformed to *z* scores) of the node pair connected by that edge. To overlay PSP-related deficits on the healthy brain graph, nodes were colored by the *t* score resulting from the 2-sample *t* test for node total flow (PSP<HC3) and thresholded at $p<0.05$, corrected for false discovery rate across the network. aINS=anterior insula; BG=basal ganglia; DentN=dentate nucleus; L=left; MFG=middle frontal gyrus; MTJ=mesothalamic junction; pACC=pregenual anterior cingulate cortex; pMCC=posterior midcingulate cortex; PreCu=precuneus; PreSMA=pre–supplementary motor area; R=right; RSC=retrosplenial cortex; Thal=thalamus.**

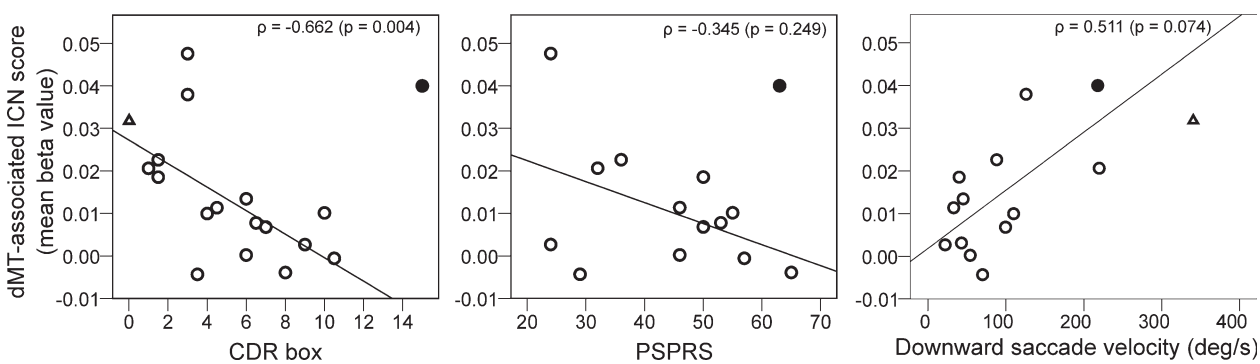


**FIGURE 5: Clinical correlations to dorsal midbrain tegmentum (dMT)-associated intrinsic connectivity network (ICN) Score. Scatterplots represent the relationships between mean network connectivity and Clinical Dementia Rating (CDR) sum of boxes score, Progressive Supranuclear Palsy Rating Scale (PSPRS), and downward saccade velocity. The dMT-associated ICN score was calculated as each subject's mean beta value across all voxels within their dMT-associated ICN map, masked by the ICN as defined in HC2 subjects (see Subjects and Methods). Circles represent progressive supranuclear palsy subjects; the filled circle indicates an outlier excluded from the CDR and PSPRS correlation analyses but included in the downward saccade velocity correlation analysis, in which she was not an outlier. For comparison, the empty triangle represents the mean dMT-associated ICN score for matched control subjects (HC3).**

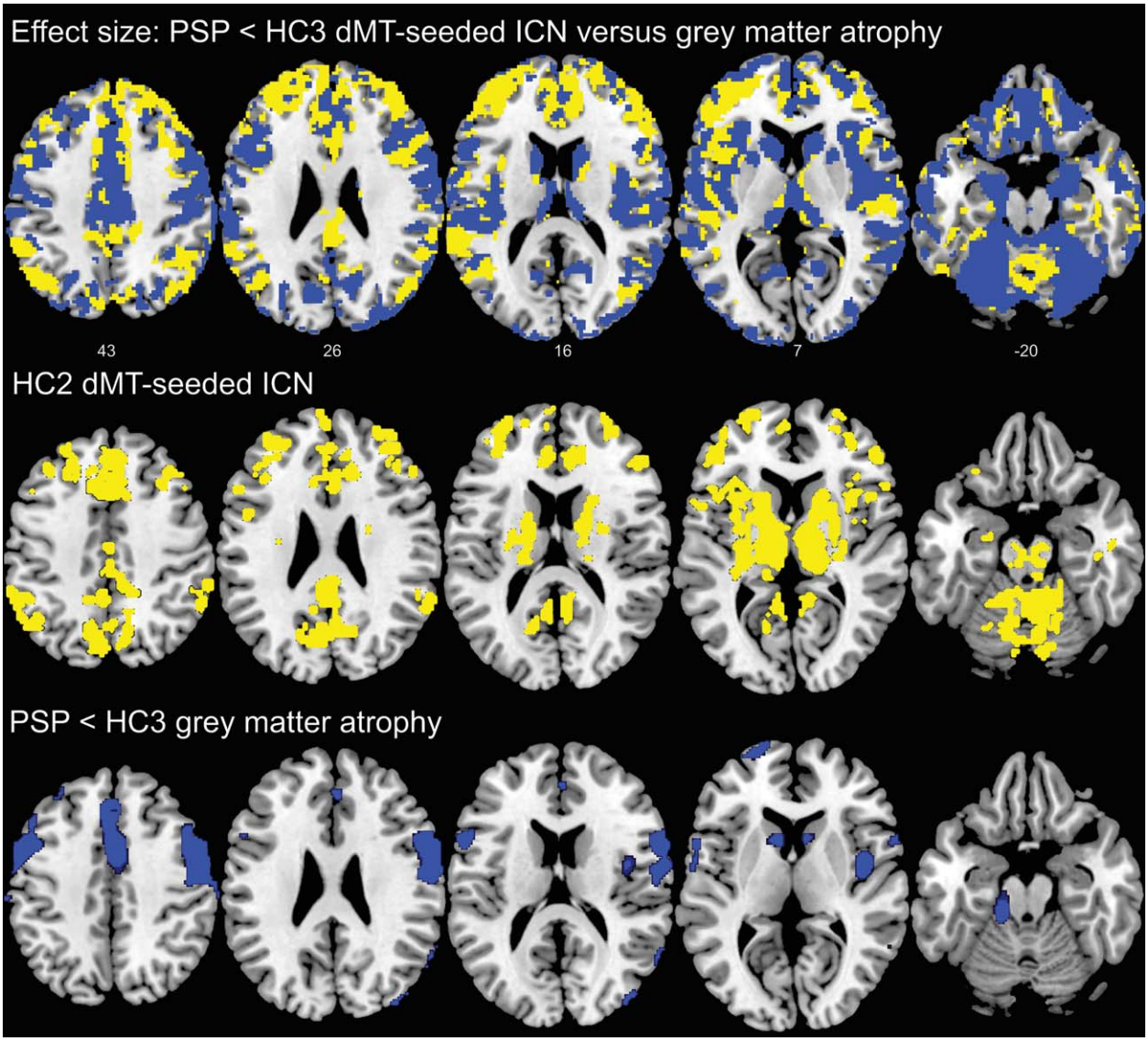


**FIGURE 6: Effect size comparison of dorsal midbrain tegmentum (dMT)-associated intrinsic connectivity network (ICN) reductions versus gray matter atrophy in patients with progressive supranuclear palsy syndrome (PSP-S) compared to matched controls. In the upper row, we compared voxelwise PSP-S<HC3 effect sizes produced by the dMT-associated ICN and voxel-based morphometry (VBM) gray matter analyses. Voxels where the dMT ICN reduction produced a greater effect size are shown in yellow, whereas voxels where VBM afforded a greater effect size are shown in blue. Effect size maps were thresholded to include only those voxels that had a moderate effect size (0.5) or greater. In the middle row, for comparison, we display the corresponding views of the dMT ICN map from the HC2 network discovery group (as shown in Fig 2; height threshold $p<0.0001$, extent threshold $p<0.001$, familywise error corrected at the cluster level). In the bottom row, the corresponding VBM gray matter atrophy pattern in PSP-S compared to HC3 ($p<0.05$, familywise error corrected at the voxel level across the whole brain) illustrates the relative structural integrity of regions where ICN methods produced greater effect sizes than VBM. Slice labels reflect Montreal Neurological Institute coordinates. The right side of the images corresponds to the right side of the brain. Note that the effect size and VBM analyses were conducted on gray matter maps, which exclude most brainstem regions.**

task-free fMRI. We further demonstrated that this method detects robust, distributed, and functionally relevant connectivity reductions in PSP-S within a network of skeletal and ocular motor control structures as well as in regions that participate in executive, social–emotional, and speech–language functions. These findings suggest that the heterogeneous clinical presentations of PSP pathology may reflect the gradient of pathology within nodes of the broader network outlined here. Patients whose disease begins in the dorsal midbrain and its closest motor control system affiliates will present with typical PSP-S but would be predicted to later develop behavioral and language deficits when pathology reaches the relevant network nodes. In contrast, patients whose pathology begins in cortical nodes may present with bvFTD, progressive nonfluent aphasia, or a corticobasal

syndrome, depending on the node and hemisphere affected first, before disease spreads along network lines to produce the defining oculomotor and gait impairments that lead clinicians to predict PSP as the underlying histopathology. Perhaps most importantly, we found that intrinsic connectivity disruption correlated with overall clinical severity and detected PSP-S–related network dysfunction in regions lacking significant gray matter atrophy.

### *Relationship of Present Findings to PSP Anatomical Literature*

Recently, Whitwell et al[39] performed a task-free fMRI analysis in patients with PSP-S. First, they performed a seed-based analysis using an ROI containing the entire bilateral thalami. Although several regions showed increased or decreased connectivity to this thalamic seed, it is difficult to place these results in an anatomical context given the diverse anatomical and intrinsic functional connections of the thalamus.[40] Second, these authors applied independent component analysis in healthy controls to identify a "basal ganglia network," which showed connectivity reductions in PSP-S compared to the same healthy controls. This strategy, using the same control subjects to select and analyze the network, reduces confidence in the reported group differences due to the problem of statistical dependency.[41] Here, we used a data-driven seed-based approach to define a reproducible dMT-associated network targeted in PSP-S compared to an independent sample of healthy controls. We observed no increases in network connectivity, perhaps reflecting the anatomical specificity of our approach.

The present work builds on a foundation of previous PSP-S neuropathological and imaging studies. Although the core pathological distribution of PSP has been recognized since the disorder's initial description,[1] more recent structural imaging and pathological analyses have shed light on the cortical vulnerability patterns associated with typical and atypical PSP.[9,17,18] Recent work using diffusion tensor imaging has underlined the role of white matter tract degeneration, especially within the superior cerebellar peduncle.[42,43] Positron emission tomography studies analyzing the covariance of metabolic patterns across patients and controls have shown a PSP-related pattern that distinguishes PSP from other atypical parkinsonian syndromes[44] and includes many of the structures identified here with ICN fMRI.[45] Overall, these investigations converge on a core set of PSP-affected structures while suggesting that the anatomical pattern relates closely to the associated clinical syndrome. The present study advances this framework by delineating a specific dMT-associated large-scale network and demonstrating that task-free fMRI detects PSP-S–related connectivity breakdowns. Our results further outline a comprehensive architecture of node pairwise connections for this system and show that PSP-S–related connectivity breakdowns emphasize cortico-subcortical and cortico-brainstem interactions and correlate with clinical severity. Although intrinsic brainstem circuits may also lose functional connectivity in PSP-S, connectivity between brainstem node pairs was less conspicuously affected in the present analyses. Whether this observation reflects PSP biology or methodological limitations requires further study.

### *Relationship of Present Findings to ICN Literature on Idiopathic Parkinson Disease*

Our PSP-S findings also fit into a context provided by a growing task-free fMRI literature on idiopathic Parkinson disease (IPD). Although some studies of patients with IPD off of dopaminergic agents have shown decreased connectivity between various cortical motor regions and basal ganglia,[46,47] others have shown increased connectivity in sensorimotor circuits, specifically between dorsal caudal putamen, inferior temporal gyrus, anterior cingulate cortex, and superior frontal gyrus. These areas of increased connectivity diminished when the patients were rescanned on dopaminergic agents.[48] Fascinating recent work[49] has suggested increased functional connectivity between the subthalamic nucleus (STN) and cortical motor areas in the off-medication state in IPD, supporting the notion of basal ganglia–thalamocortical circuit hypersynchronicity in IPD[50] and providing a possible mechanism for STN-targeted deep brain stimulation. In contrast to the IPD findings, the matrix analysis performed here suggested decreased connectivity between thalamus, basal ganglia, and pre-SMA in PSP-S, although half of the patients were not taking dopaminergic agents at the time of scanning. This contrast to IPD could reflect the severe STN tau pathology in PSP and explain, at least in part, why most patients with PSP-S do not respond to L-dopa or STN deep brain stimulation treatment[51] and why we found no significant difference in mean dMT-associated network connectivity between patients on and off dopaminergic agents.

### *Insights Revealed by Matrix and Graph Theoretical Analyses*

Networks represent multiple nodal interactions between spatially distributed and functionally diverse regions. Seed-based ICN analysis can identify regions with abnormal connectivity to a chosen network node such as, in this case, the dMT. Although this method works well for network identification, it provides no information about

how network nodes interact with regions other than the seed. Including matrix and graph theoretical analyses enabled us to delineate the healthy dMT-associated network configuration and identify its hublike nodes in the mesothalamic junction, basal ganglia, and thalamus. These nodes may serve as PSP-vulnerable network epicenters whose connectivity patterns predict degeneration severity throughout the network, as shown for other neurodegenerative disease syndromes.[52] Graph theoretical analyses revealed PSP-S–related reductions in nodal network traffic (total flow) and local interconnectivity (clustering coefficient). Additional work is needed to determine whether characterizing the healthy brain functional connectome can predict the pace and topography of progression in single patients with PSP-S and other neurodegenerative syndromes.

### *Clinical Correlation*

In PSP-S, a dMT-associated ICN summary score correlated with the CDR sum of boxes score, a measure of overall clinical severity. Similar but weaker correlations with the UPDRS, PSPRS, and downward saccade velocity may have escaped significance due to the smaller samples for which these data were available or because these measures sample too narrow a range of PSP-S–related deficits to correlate with average network connectivity. The outlier uncovered in these analyses had the fastest downward saccades within the PSP-S group, consistent with this patient's high dMT-ICN score. These observations raise important questions, including whether this patient has a non-PSP neuropathology, represents an atypical midbrain-sparing PSP presentation, or reflects method-related statistical noise. Despite these lingering questions, our cross-sectional findings suggest that ICN mapping merits further investigation as a potential disease-monitoring biomarker for longitudinal studies and treatment trials.

### *Sensitivity of Intrinsic Connectivity Analysis to Early Stage Network Degeneration*

ICN analysis outperformed VBM in discriminating PSP-S from controls in network regions that lacked significant group-level atrophy. This finding hints at a potential role for ICN analysis in detecting early PSP-S–related changes. Longitudinal studies are needed to determine whether ICN data provide the "leading edge," sensitive to early network dysfunction and predicting where atrophy will emerge next. This capability would provide a much-needed index of early stage disease for patients genetically at risk for PSP or other neurodegenerative diseases, especially once potential disease-modifying therapies enter clinical trials.

### *Limitations and Future Directions*

This study focused on identifying a PSP-related ICN using novel network mapping methods. The analysis was not designed to provide a comprehensive multimodal neuroimaging comparison or to use imaging to predict pathology. Although the typical PSP syndrome we studied strongly predicts PSP pathology,[25] some patients in this study could have had a non-PSP histopathology, and future studies are needed to determine whether ICN measurements can single out patients with PSP-S who lack PSP pathology. Many patients studied here took medications to address ongoing motor or psychiatric/behavioral symptoms. These medications could have influenced the ICN results, yet studying only medication-free patients with PSP-S would have proven unfeasible even at our referral center, where recruiting patients with PSP-S represents a major research priority. The noninvasive and repeatable nature of ICN methods makes them attractive potential longitudinal biomarkers, and future work should explore this potential by studying patients with PSP and other network-based neurodegenerative disorders over time.

## Acknowledgment

This work was supported by the Tau Consortium (A.L.B., B.L.M., W.W.S.), Larry L. Hillblom Foundation (J.H.K., B.L.M.), Shupin Foundation (R.C.G.), CurePSP (A.L.B.), Association for Frontotemporal Degeneration (A.L.B.), Allon Therapeutics (A.L.B.), and NIH (National Institute on Aging grants AG023501 to B.L.M. and W.W.S., AG031278 and AG038791 to A.L.B., AG032289 to J.H.K., AG1657303 to B.L.M.).

We thank Dr. M. Milham and colleagues at NYU School of Medicine for providing public access to the young control fMRI data set used here; and our patients and their families for their invaluable contributions to neurodegenerative disease research.

## Authorship

R.C.G., A.L.B., and A.T. made equal contributions.

## Potential Conflicts of Interest

A.L.B.: consultancy, Plexxikon, Phloronol, BMS, Registrat-Mapi, Genentech, Allon Therapeutics; grants/grants pending, BMS, Elan, Allon Therapeutics, Association for Frontotemporal Degeneration, Alzheimer's Drug Discovery Foundation, Hellman Family Foundation, Silicon Valley Foundation, Agouron Institute, Pfizer, Janssen, Forest, Medivation. B.L.M.: board membership, John Douglas French Alzheimer's Foundation, Larry L. Hillblom Foundation; consultancy, TauRx, Allon Therapeutics; grants/grants pending, Novartis. W.W.S.: grants/

grants pending, National Institute on Aging, John D. French Alzheimer's Disease Foundation, Consortium for Frontotemporal Dementia Research, James S. McDonnell Foundation, Larry L. Hillblom Foundation; speaking fees, Alzheimer's Association, American Academy of Neurology, Novartis Korea; travel expenses, Alzheimer's Association.

## References


1. Steele JC, Richardson JC, Olszewski J. Progressive Supranuclear Palsy. Arch Neurol 1964;10:333–360.
2. Josephs KA, Petersen RC, Knopman DS, et al. Clinicopathologic analysis of frontotemporal and corticobasal degenerations and PSP. Neurology 2006;66:41–48.
3. Dubois B, Pillon B, Legault F, et al. Slowing of cognitive processing in progressive supranuclear palsy. A comparison with Parkinson's disease. Arch Neurol 1988;45:1194–1199.
4. Pillon B, Blin J, Vidailhet M, et al. The neuropsychological pattern of corticobasal degeneration: comparison with progressive supranuclear palsy and Alzheimer's disease. Neurology 1995;45:1477–1483.
5. Bak TH, Crawford LM, Hearn VC, et al. Subcortical dementia revisited: similarities and differences in cognitive function between progressive supranuclear palsy (PSP), corticobasal degeneration (CBD) and multiple system atrophy (MSA). Neurocase 2005;11:268–273.
6. Aarsland D, Litvan I, Larsen JP. Neuropsychiatric symptoms of patients with progressive supranuclear palsy and Parkinson's disease. J Neuropsychiatry Clin Neurosci 2001;13:42–49.
7. Schofield EC, Hodges JR, Macdonald V, et al. Cortical atrophy differentiates Richardson's syndrome from the parkinsonian form of progressive supranuclear palsy. Mov Disord 2011;26:256–263.
8. Hauw JJ, Daniel SE, Dickson D, et al. Preliminary NINDS neuropathologic criteria for Steele-Richardson-Olszewski syndrome (progressive supranuclear palsy). Neurology 1994;44:2015–2019.
9. Dickson DW, Ahmed Z, Algom AA, et al. Neuropathology of variants of progressive supranuclear palsy. Curr Opin Neurol 2010;23:394–400.
10. Mackenzie IR, Neumann M, Bigio EH, et al. Nomenclature and nosology for neuropathologic subtypes of frontotemporal lobar degeneration: an update. Acta Neuropathol 2010;119:1–4.
11. Salmon E, Van der Linden MV, Franck G. Anterior cingulate and motor network metabolic impairment in progressive supranuclear palsy. Neuroimage 1997;5:173–178.
12. Saper CB, Wainer BH, German DC. Axonal and transneuronal transport in the transmission of neurological disease: potential role in system degenerations, including Alzheimer's disease. Neuroscience 1987;23:389–398.
13. Chen AL, Riley DE, King SA, et al. The disturbance of gaze in progressive supranuclear palsy: implications for pathogenesis. Front Neurol 2010;1:147.
14. Fox MD, Raichle ME. Spontaneous fluctuations in brain activity observed with functional magnetic resonance imaging. Nat Rev Neurosci 2007;8:700–711.
15. Seeley WW, Crawford RK, Zhou J, et al. Neurodegenerative diseases target large-scale human brain networks. Neuron 2009;62:42–52.
16. Buckner RL, Snyder AZ, Shannon BJ, et al. Molecular, structural, and functional characterization of Alzheimer's disease: evidence for a relationship between default activity, amyloid, and memory. J Neurosci 2005;25:7709–7717.
17. Boxer AL, Geschwind MD, Belfor N, et al. Patterns of brain atrophy that differentiate corticobasal degeneration syndrome from progressive supranuclear palsy. Arch Neurol 2006;63:81–86.
18. Josephs KA, Whitwell JL, Dickson DW, et al. Voxel-based morphometry in autopsy proven PSP and CBD. Neurobiol Aging 2008;29:280–289.
19. Habas C, Kamdar N, Nguyen D, et al. Distinct cerebellar contributions to intrinsic connectivity networks. J Neurosci 2009;29:8586–8594.
20. Cummings JL, Benson DF. Subcortical dementia. Review of an emerging concept. Arch Neurol 1984;41:874–879.
21. Foster NL, Gilman S, Berent S, et al. Cerebral hypometabolism in progressive supranuclear palsy studied with positron emission tomography. Ann Neurol 1988;24:399–406.
22. Shehzad Z, Kelly AM, Reiss PT, et al. The resting brain: unconstrained yet reliable. Cereb Cortex 2009;19:2209–2229.
23. Rosen HJ, Gorno-Tempini ML, Goldman WP, et al. Patterns of brain atrophy in frontotemporal dementia and semantic dementia. Neurology 2002;58:198–208.
24. Boxer AL, Garbutt S, Seeley WW, et al. Saccade abnormalities in autopsy-confirmed frontotemporal lobar degeneration and Alzheimer disease. Arch Neurol 2012;69:509–517.
25. Litvan I, Agid Y, Calne D, et al. Clinical research criteria for the diagnosis of progressive supranuclear palsy (Steele-Richardson-Olszewski syndrome): report of the NINDS-SPSP international workshop. Neurology 1996;47:1–9.
26. Golbe LI, Ohman-Strickland PA. A clinical rating scale for progressive supranuclear palsy. Brain 2007;130(pt 6):1552–1565.
27. Van Dijk KR, Sabuncu MR, Buckner RL. The influence of head motion on intrinsic functional connectivity MRI. Neuroimage 2012;59:431–438.
28. Guo CC, Kurth F, Zhou J, et al. One-year test-retest reliability of intrinsic connectivity network fMRI in older adults. Neuroimage 2012;61:1471–1483.
29. Churchill NW, Oder A, Abdi H, et al. Optimizing preprocessing and analysis pipelines for single-subject fMRI. I. Standard temporal motion and physiological noise correction methods. Hum Brain Mapp 2012;33:609–627.
30. Biswal BB, Mennes M, Zuo XN, et al. Toward discovery science of human brain function. Proc Natl Acad Sci U S A 2010;107:4734–4739.
31. Allen EA, Erhardt EB, Damaraju E, et al. A baseline for the multivariate comparison of resting-state networks. Front Syst Neurosci 2011;5:2.
32. Casanova R, Srikanth R, Baer A, et al. Biological parametric mapping: a statistical toolbox for multimodality brain image analysis. Neuroimage 2007;34:137–143.
33. Poline JB, Worsley KJ, Evans AC, Friston KJ. Combining spatial extent and peak intensity to test for activations in functional imaging. Neuroimage 1997;5:83–96.
34. Zhou J, Greicius MD, Gennatas ED, et al. Divergent network connectivity changes in behavioural variant frontotemporal dementia and Alzheimer's disease. Brain 2010;133(pt 5):1352–1367.
35. Bullmore E, Sporns O. Complex brain networks: graph theoretical analysis of structural and functional systems. Nat Rev Neurosci 2009;10:186–198.
36. Rubinov M, Sporns O. Complex network measures of brain connectivity: uses and interpretations. Neuroimage 2010;52:1059–1069.
37. Seeley WW, Crawford R, Rascovsky K, et al. Frontal paralimbic network atrophy in very mild behavioral variant frontotemporal dementia. Arch Neurol 2008;65:249–255.

38. Nestor PJ, Graham NL, Fryer TD, et al. Progressive non-fluent aphasia is associated with hypometabolism centred on the left anterior insula. Brain 2003;126(pt 11):2406–2418.

39. Whitwell JL, Avula R, Master A, et al. Disrupted thalamocortical connectivity in PSP: a resting-state fMRI, DTI, and VBM study. Parkinsonism Relat Disord 2011;17:599–605.

40. Kim DJ, Park B, Park HJ. Functional connectivity-based identification of subdivisions of the basal ganglia and thalamus using multilevel independent component analysis of resting state fMRI. Hum Brain Mapp 2012 Feb 14.

41. Kriegeskorte N, Simmons WK, Bellgowan PS, Baker CI. Circular analysis in systems neuroscience: the dangers of double dipping. Nat Neurosci 2009;12:535–540.

42. Canu E, Agosta F, Baglio F, et al. Diffusion tensor magnetic resonance imaging tractography in progressive supranuclear palsy. Mov Disord 2011;26:1752–1755.

43. Whitwell JL, Master AV, Avula R, et al. Clinical correlates of white matter tract degeneration in progressive supranuclear palsy. Arch Neurol 2011;68:753–760.

44. Tang CC, Poston KL, Eckert T, et al. Differential diagnosis of parkinsonism: a metabolic imaging study using pattern analysis. Lancet Neurol 2010;9:149–158.

45. Eckert T, Tang C, Ma Y, et al. Abnormal metabolic networks in atypical parkinsonism. Mov Disord 2008;23:727–733.

46. Wu T, Long X, Wang L, et al. Functional connectivity of cortical motor areas in the resting state in Parkinson's disease. Hum Brain Mapp 2011;32:1443–1457.

47. Helmich RC, Derikx LC, Bakker M, et al. Spatial remapping of cortico-striatal connectivity in Parkinson's disease. Cereb Cortex 2010;20:1175–1186.

48. Kwak Y, Peltier S, Bohnen NI, et al. Altered resting state cortico-striatal connectivity in mild to moderate stage Parkinson's disease. Front Syst Neurosci 2010;4:143.

49. Baudrexel S, Witte T, Seifried C, et al. Resting state fMRI reveals increased subthalamic nucleus-motor cortex connectivity in Parkinson's disease. Neuroimage 2011;55:1728–1738.

50. Hammond C, Bergman H, Brown P. Pathological synchronization in Parkinson's disease: networks, models and treatments. Trends Neurosci 2007;30:357–364.

51. van Balken I, Litvan I. Current and future therapeutic approaches in progressive supranuclear palsy. Handb Clin Neurol 2008;89:493–508.

52. Zhou J, Gennatas ED, Kramer JH, et al. Predicting regional neurodegeneration from the healthy brain functional connectome. Neuron 2012;73:1216–1227.